



## Assessing of Photoluminescence and Structural Properties of Dy<sup>3+</sup> doped Cadmium Tantalate Phosphor on the Basis of Charge Balance

### Dy<sup>3+</sup> Katkılı Kadmiyum Tantalat Fosforunun Fotolüminesans ve Yapısal Özelliklerinin Yük Dengesi Temelinde Değerlendirilmesi

Lütfiye Feray Güleriyüz<sup>✉</sup>

Department of Mechanical Engineering, Ege University, Bornova, 35040, İzmir, Turkey.

#### ABSTRACT

Based on the charge balance, trivalent dysprosium doped Cd<sub>1-x</sub>Ta<sub>2</sub>O<sub>6</sub>:xDy<sup>3+</sup> (x=0.5, 1, 2, 3, 5 at%) phosphor series was fabricated by solid state reaction route at 1100 °C for 8 h. The synthesized phosphors were investigated by XRD (X-ray diffraction), SEM (scanning electron microscopy), and PL (photoluminescence) analyses. XRD and SEM analyzes revealed the orthorhombic colombite crystal structure and the presence of oval-like and shapeless morphology with submicron and several micron grain sizes, respectively. With the excitation of 387.8 nm, the phosphors exhibited blue and yellow emissions at 482.4 nm and 578.5 nm depending on the <sup>4</sup>F<sub>9/2</sub>→<sup>6</sup>H<sub>15/2</sub> and <sup>4</sup>F<sub>9/2</sub>→<sup>6</sup>H<sub>13/2</sub> transitions of Dy<sup>3+</sup>, respectively. The emission intensity of cadmium tantalate phosphor increased with increasing Dy<sup>3+</sup> concentration up to x=5 at% value, and did not occurred the concentration quenching which reduces emission intensity. The reason why concentration quenching did not occur can be attributed to the reduction of structural defects due to the improvement in charge balance and the reduction of the conversion of excitation energy to nonradiative transitions. The Commission Internationale d'Eclairage (CIE) coordinates of Cd<sub>1-x</sub>Ta<sub>2</sub>O<sub>6</sub>:xDy<sup>3+</sup> (x=0.5, 1, 2, 3, 5 at%) phosphors were found near the white region in the chromaticity diagram.

#### Key Words

Photoluminescence, XRD, SEM, W-LEDs.

#### ÖZ

Yük dengesine dikkate alınarak, trivalent disprosium katkılı Cd<sub>1-x</sub>Ta<sub>2</sub>O<sub>6</sub>:xDy<sup>3+</sup> (x=%0.5, 1, 2, 3, 5 at) fosfor serisi katı hal reaksiyonu yolu ile 1100 °C 'de 8 saat süreyle üretilmiştir. Sentezlenen fosforlar XRD (X-ışını kırınımı), SEM (taramalı elektron mikroskobu) ve PL (fotolüminesans) analizleri ile incelenmiştir. XRD ve SEM analizleri ortorombik kolombit kristal yapısını ve sırasıyla mikron altı ve birkaç mikron tane boyutuna sahip oval benzeri ve şekilsiz morfolojinin varlığını ortaya çıkardı. 387.8 nm'lik uyarım ile fosforlar, Dy<sup>3+</sup> 'nin <sup>4</sup>F<sub>9/2</sub>→<sup>6</sup>H<sub>15/2</sub> and <sup>4</sup>F<sub>9/2</sub>→<sup>6</sup>H<sub>13/2</sub> geçişlerine bağlı olarak sırasıyla 482.4 nm ve 578.5 nm'de mavi ve sarı emisyonlar sergilediler. Kadmiyum tantalat fosforun emisyon şiddeti Dy<sup>3+</sup> konsantrasyonu ile x=%5 at değerine kadar artarken emisyon şiddetinin azaltan konsantrasyon söndürme gerçekleşmemiştir. Konsantrasyon söndürmenin meydana gelmemesinin sebebi yük dengesindeki iyileşme nedeniyle yapısal kusurların azalması ve uyarma enerjisinin ışınımsız geçişlere dönüşümünün azalmasına bağlanabilir. Cd<sub>1-x</sub>Ta<sub>2</sub>O<sub>6</sub>:xDy<sup>3+</sup> (x=%0.5, 1, 2, 3, 5 at) fosforlarının Commission Internationale d'Eclairage (CIE) koordinatları kromatiklik diyagramında beyaz bölgenin yakınında bulunmuştur.

#### Anahtar Kelimeler

Fotolüminesans, XRD, SEM, W-LEDs.

**Article History:** Received: Jan 13, 2022; Revised: Mar 10, 2022; Accepted: Mar 10, 2022; Available Online: Jul 5, 2022.

**DOI:** <https://doi.org/10.15671/hjbc.1056363>

**Correspondence to:** L. F. Güleriyüz, Ege University, Bornova, 35040, İzmir, Turkey.

**E-Mail:** ferayguleryuz@hotmail.com

## INTRODUCTION

The cadmium contained quantum dots (QDs) have attracted enormous interests in the last decade as a novel class of material due to their special properties and a wide area of potential applications such as biomedical screening, light-emitting diodes (LEDs), solar cells, optics, and biosensors [1-5]. On the other hand, the inherent toxicity of cadmium limits its applications, especially in the biomedical and industrial areas. For example, the cytotoxicity and genotoxicity of QDs with a Cadmium selenide/Zinc sulfide (CdSe/ZnS) core/shell for applications in cancer therapy has been discussed recently [6]. However, cadmium-based phosphors have been put into use recently since they provide high levels of brightness. This leads to a reduction in the need for high levels of X-ray doses. Accordingly, the risk of health problems can be minimized [1,7].

Trivalent RE<sup>3+</sup> ions with 4f–4f inner-shell transitions possess specific advantage features such as high luminescence yield, narrow emission line, and long decay time constant. Hence, rare earth (RE<sup>3+</sup>) doped materials have wide range of applications in the field of solid state lighting, display, and laser technologies. Moreover, in recent years, white light emitting diodes (W-LEDs) have been targeted as next generation solid state lighting sources due to the advantages of energy saving, high efficiency, long lifetime, reliability and environmentally friendly properties [8-18]. Trivalent dysprosium (Dy<sup>3+</sup>) doped phosphors are of great attention due to white light emission property. As RE<sup>3+</sup> metals, Dy<sup>3+</sup> has two dominant emission bands: one is in blue region (470–500 nm) due to <sup>4</sup>F<sub>9/2</sub> → <sup>6</sup>H<sub>15/2</sub> transition and the other is in yellow region (570–600 nm) corresponding to the <sup>4</sup>F<sub>9/2</sub> → <sup>6</sup>H<sub>13/2</sub> transition [1-7].

The crystal structure of CdTa<sub>2</sub>O<sub>6</sub> is expressed by ternary oxides of the general formula AB<sub>2</sub>O<sub>6</sub> (A=M<sup>2+</sup>, B=Nb, Ta). In the AB<sub>2</sub>O<sub>6</sub> columbite structure, the A and B cations are at the center of octahedral surrounded by six oxygen atoms. The AO<sub>6</sub> and BO<sub>6</sub> octahedra form independent zig-zag chains by sharing edges, and the chains are connected by sharing corners in the order AO<sub>6</sub> chain-BO<sub>6</sub> chain-BO<sub>6</sub> chain [8,15]. Cadmium tantalate has been investigated due to photocatalytic [19] neutron absorption and [20] photoluminescence properties [8,15].

Photoluminescence of CdTa<sub>2</sub>O<sub>6</sub>:Dy<sup>3+</sup> phosphor has

been previously reported in the literature in which the highest luminescence was obtained for 1 mol% Dy<sup>3+</sup> doped sample [8]. In the study, the effect of charge balance of Dy<sup>3+</sup> doped Cd<sub>1-x</sub>Ta<sub>2</sub>O<sub>6</sub>:xDy<sup>3+</sup> (x=0.5, 1, 2, 3, 5 at%) phosphors was investigated on the structural and photoluminescence properties. The structural characterization and photoluminescence properties of the samples were performed using the SEM, XRD, EDS and fluorometric analyses.

## MATERIALS and METHODS

Undoped and Cd<sub>1-x</sub>Ta<sub>2</sub>O<sub>6</sub>:xDy<sup>3+</sup> (x=0.5, 1, 2, 3, 5 at% or x=0.25, 0.5, 1, 1.5, 2.5 mol% Dy<sub>2</sub>O<sub>3</sub>) materials were synthesized by a solid state reaction method. Cd(NO<sub>3</sub>)<sub>2</sub>·4H<sub>2</sub>O with purity of 99% (Sigma-Aldrich) and Ta<sub>2</sub>O<sub>5</sub> with purity of 99.9% (Alfa Aesar) powders were used as starting materials. Dy<sub>2</sub>O<sub>3</sub> with purity of 99.9% (Alfa Aesar) was used as a dopant. The Cd(NO<sub>3</sub>)<sub>2</sub>·4H<sub>2</sub>O, Ta<sub>2</sub>O<sub>5</sub> and Dy<sub>2</sub>O<sub>3</sub> powders were prepared according to stoichiometry; CdTa<sub>2</sub>O<sub>6</sub>, and Cd<sub>0.995</sub>Dy<sub>0.005</sub>Ta<sub>2</sub>O<sub>6</sub>, Cd<sub>0.99</sub>Dy<sub>0.01</sub>Ta<sub>2</sub>O<sub>6</sub>, Cd<sub>0.98</sub>Dy<sub>0.02</sub>Ta<sub>2</sub>O<sub>6</sub>, Cd<sub>0.97</sub>Dy<sub>0.03</sub>Ta<sub>2</sub>O<sub>6</sub>, Cd<sub>0.95</sub>Dy<sub>0.05</sub>Ta<sub>2</sub>O<sub>6</sub>. Then Dy<sup>3+</sup> doped powder mixtures were homogenized in an agate mortar, and were sintered at 1100 °C for 8 h under air atmosphere in an electric furnace. The phase compositions and crystallography parameters in sintered samples were investigated by XRD ((XRD, Rigaku Corp., D-MAX 2200), using Cu-Kα radiation between 2θ=20–65° at 2°/min and Ni filter. The morphology and elemental composition of the sintered powders were investigated by Scanning electron microscopy (SEM, JEOL Ltd., JSM-5910LV) and PL (photoluminescence) analyses. , excitation and emission spectra were recorded by using a Scinco fluoromaster-FS/2 model fluorometer with a Xe-arc lamp (150 W) as excitation source. PL analysis were carried out under room temperature

## RESULTS and DISCUSSION

### Structural analysis

Figure 1 shows XRD results of Cd<sub>1-x</sub>Ta<sub>2</sub>O<sub>6</sub>:xDy<sup>3+</sup> (x=0.5, 1, 2, 3, 5 at) samples at 1100 for 8h. XRD analysis shows that Cd<sub>1-x</sub>Ta<sub>2</sub>O<sub>6</sub>:xDy<sup>3+</sup> samples crystallized in orthorhombic symmetry (JCPDS card No.39-1431) with space group Pbcn(60) the columbite type structure. As seen from XRD pattern, the single phase structure was preserved up to the highest Dy<sup>3+</sup> concentration (x=5 at%). On the basis of the ion radius and coordination number (CN), the formation of the single-phase can be attributed to the substitution of Dy<sup>3+</sup> ions with ionic radius 0.912 Å (for 6 C.N) by Cd<sup>2+</sup> ions (r=0.95 Å, for C.N. 6). Consequently, the charge balance of

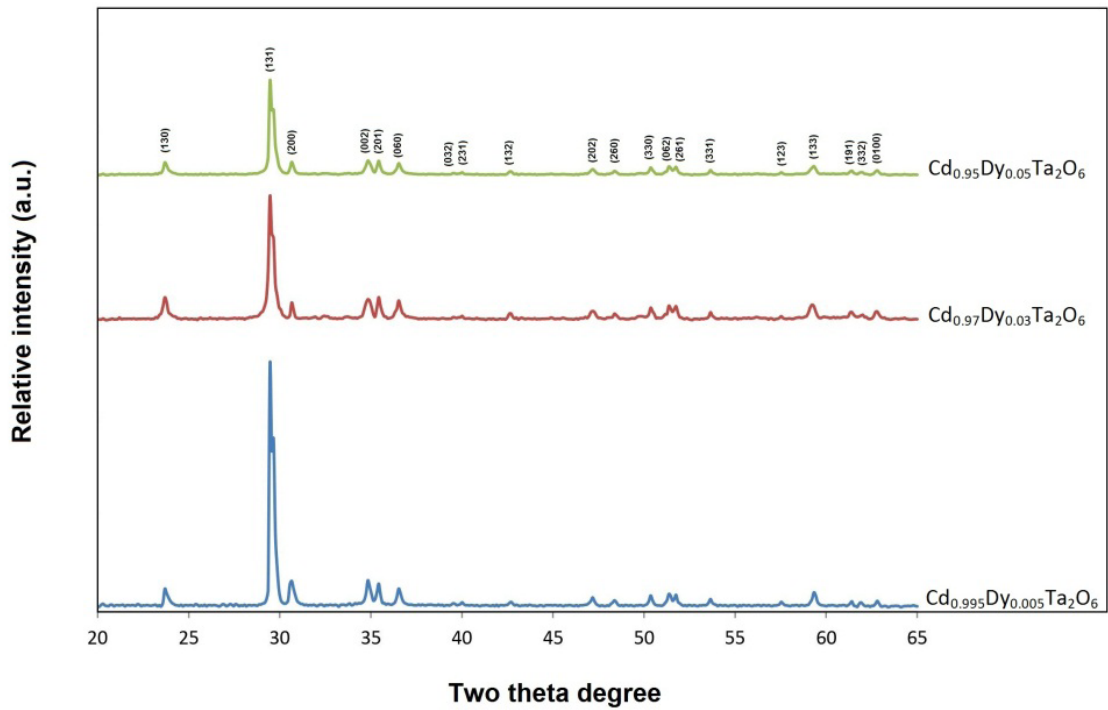


**Figure 1.** X-ray diffraction pattern of  $\text{Cd}_{0.995}\text{Dy}_{0.005}\text{Ta}_2\text{O}_6$ ,  $\text{Cd}_{0.97}\text{Dy}_{0.03}\text{Ta}_2\text{O}_6$  and  $\text{Cd}_{0.95}\text{Dy}_{0.05}\text{Ta}_2\text{O}_6$  samples.

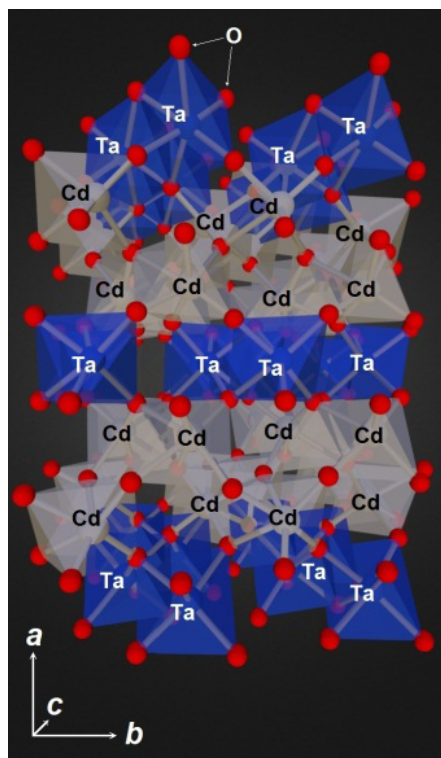


**Figure 2.** Schematic illustration of orthorhombic columbite crystal structure in the direction of b axis

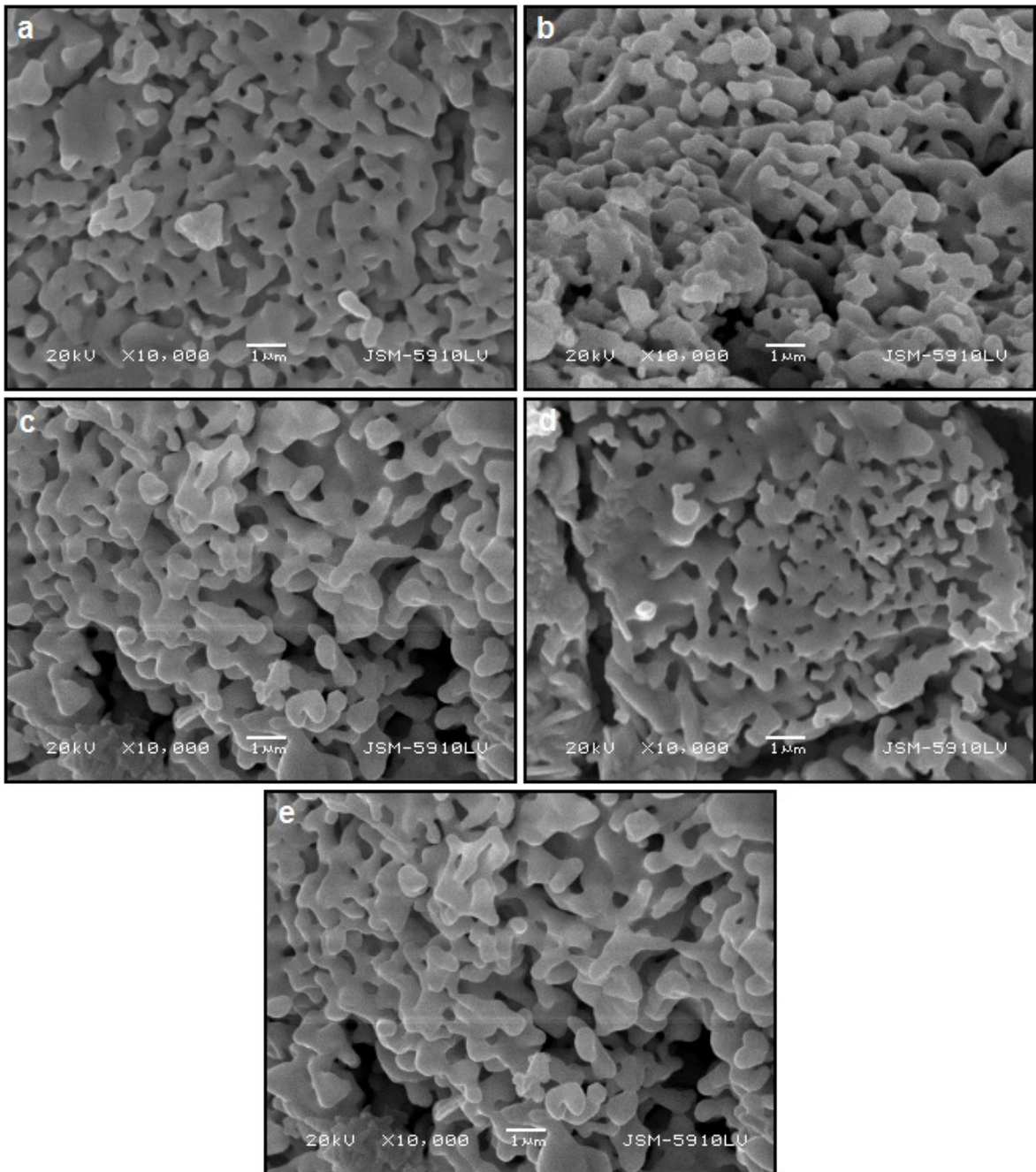


**Figure 3.** SEM micrographs of  $Cd_{1-x}Ta_2O_6:xDy^{3+}$  powders; (a) undoped or  $x=0$ , (b)  $x=0.5$ , (c)  $x=1$ , (d)  $x=3$  and (e)  $x=5$ .

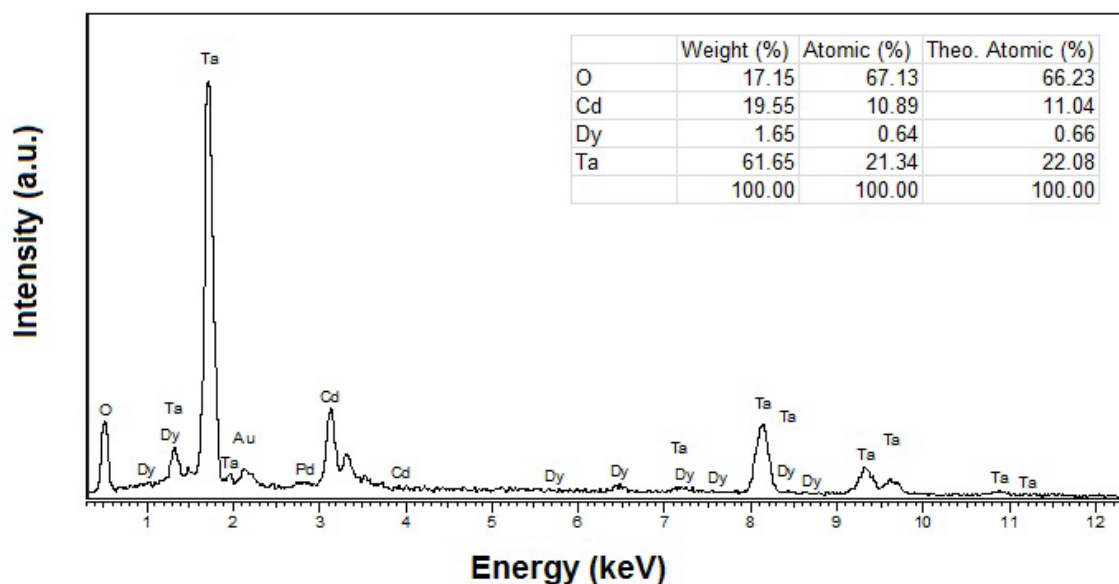


**Figure 4.** EDS spectrum and elemental amounts (wt%, at% and theoretical%) of  $\text{Cd}_{0.97}\text{Dy}_{0.03}\text{Ta}_2\text{O}_6$  sample

the structure may vary slightly, but the orthorhombic symmetry of the lattice prevented up to  $x=5$  at% concentration. The orthorhombic columbite crystal structure could be illustrated as shown in Figure 2.

Figure 3 (a-e) shows the SEM micrographs of  $\text{CdTa}_2\text{O}_6$  (a),  $\text{Cd}_{0.995}\text{Dy}_{0.005}\text{Ta}_2\text{O}_6$  (b),  $\text{Cd}_{0.99}\text{Dy}_{0.01}\text{Ta}_2\text{O}_6$  (c),  $\text{Cd}_{0.97}\text{Dy}_{0.03}\text{Ta}_2\text{O}_6$  (d),  $\text{Cd}_{0.95}\text{Dy}_{0.05}\text{Ta}_2\text{O}_6$  (e) powders were sintered at  $1100^\circ\text{C}$  for 8 h. The grain morphology of the samples is oval and shapeless. As seen in the SEM micrographs, the increased in  $\text{Dy}^{3+}$  concentration did not cause any notable changes in shape and grain size. Figure 4 shows EDS spectrum and elemental compositions of  $\text{Cd}_{0.97}\text{Dy}_{0.03}\text{Ta}_2\text{O}_6$  sample. The elemental compositions (weight%, atomic%) of O, Cd, Dy, Ta are compatible with the theoretical compositions.

#### Photoluminescence analysis

Figure 5 shows the excitation spectra of  $\text{Cd}_{1-x}\text{Ta}_2\text{O}_6:x\text{Dy}^{3+}$  ( $x=0.5, 1, 2, 3, 5$  at%) phosphors monitored at  $579.2\text{ nm}$ . The excitation spectra in the range of  $300\text{--}420\text{ nm}$  belong to between the ground level and the  ${}^6\text{H}_{15/2} \rightarrow {}^4\text{M}_{17/2}$  ( $326.2\text{ nm}$ ),  ${}^6\text{H}_{15/2} \rightarrow {}^4\text{F}_{5/2}$  ( $339.3\text{ nm}$ ),  ${}^6\text{H}_{15/2} \rightarrow {}^6\text{P}_{7/2}$  ( $352.2\text{ nm}$ ),  ${}^6\text{H}_{15/2} \rightarrow {}^4\text{P}_{3/2}$  ( $366.0\text{ nm}$ ), and  ${}^6\text{H}_{15/2} \rightarrow {}^4\text{I}_{13/2}$  ( $387.9\text{ nm}$ ) transitions. The emission spectra of the phosphors exhibited two emission peaks with the  ${}^4\text{F}_{9/2} \rightarrow {}^6\text{H}_{15/2}$  ( $484.5\text{ nm}$ ) and  ${}^4\text{F}_{9/2} \rightarrow {}^6\text{H}_{15/2}$  ( $579.2\text{ nm}$ ) transitions are given in Figure 6. The emission of  $\text{Dy}^{3+}$  doped  $\text{CdTa}_2\text{O}_6$  samples increased by the increasing of  $\text{Dy}^{3+}$  concentration up to  $x=5$  at%, and not occurred the concentration quenching which causes a decrease in luminescence. However, in the previously reported  $\text{CdTa}_2\text{O}_6:\text{Dy}^{3+}$  study [8], the emission of  $\text{Dy}^{3+}$  doped  $\text{CdTa}_2\text{O}_6$  samples decreased over 1 mol%. In the study, the increase of PL emission up to  $x=5$  at% can be explained with the improvement in the charge balance where the structural stress and impurity phase formation decreased, and thus, the conversion of excitation energy to radiative transitions has increased.

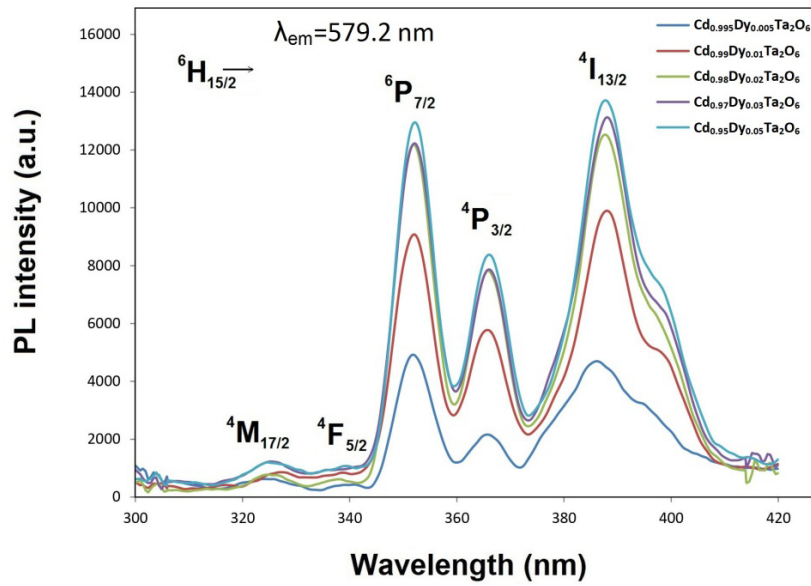


Figure 5. Excitation spectra of Cd<sub>1-x</sub>Ta<sub>2</sub>O<sub>6</sub>:xDy<sup>3+</sup> (x=0.5, 1, 2, 3, 5 at%) phosphors monitored at λ<sub>em</sub>=579.2 nm.

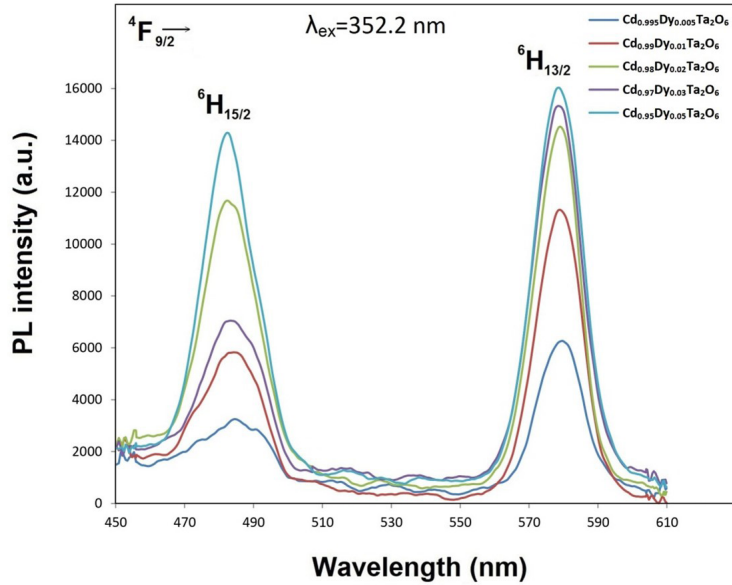


Figure 6. Emission spectra of spectra of Cd<sub>1-x</sub>Ta<sub>2</sub>O<sub>6</sub>:xDy<sup>3+</sup> (x=0.5, 1, 2, 3, 5 at%) phosphors excited at λ<sub>ex</sub>=352.2 nm.

$$R_c = 2 \left( \frac{3V}{4\pi X_c N} \right)^{1/3} \tag{1}$$

In addition, the transfer of excitation energy varies depending on the distance of Dy<sup>3+</sup>-Dy<sup>3+</sup> ions. The increase of RE<sup>3+</sup> concentration decreases between Dy<sup>3+</sup>-Dy<sup>3+</sup> and causes the increase of the non-radiative energy transfer between ions. So that, the decreasing distance between Dy<sup>3+</sup>-Dy<sup>3+</sup> ions would be promoted nonradiative energy transfer. Accordingly, the critical distance ( $R_c$ ) for the non-radiative energy transfer between Dy<sup>3+</sup>-Dy<sup>3+</sup> ions estimates from the Blasse’s equation (1) [21]:

where  $V$  is the unit cell volume,  $N$  is the number of available sites for dopant ion and  $X_c$  is the critical concentration of dopant ion. For Cd<sub>0.95</sub>Dy<sub>0.05</sub>Ta<sub>2</sub>O<sub>6</sub> phosphor, it is  $X_c=0.05$  ion (for 5 at%) in the unit cell,  $V=445.2$  (Å)<sup>3</sup> and  $N=4$ . Accordingly, the critical distance of energy transfer ( $R_c$ ) for Dy<sup>3+</sup>-Dy<sup>3+</sup> ions was calculated as 16.2 (Å). Based on Blasse’s theory [22], since the Dy<sup>3+</sup>-Dy<sup>3+</sup> distance is larger than 5 (Å), the effective mechanism will be the multipolar interaction or the mechanism of exchange interaction will ineffective.

### White light properties

The Commission Internationale de l'Éclairage (CIE) chromaticity coordinates of  $\text{Cd}_{1-x}\text{Ta}_2\text{O}_6:\text{xDy}^{3+}$  ( $x=0.5, 1, 2, 3, 5$  at%) phosphors with different doping concentrations under excitation at 352.2 nm are shown in Figure 7. The chromaticity coordinates were determined based on their corresponding PL spectra for different concentrations in the CIE chromaticity diagram is tabulated in Table 1. It is seen that the chromaticity coordinates, for all concentrations of  $\text{Cd}_{1-x}\text{Ta}_2\text{O}_6:\text{xDy}^{3+}$  ( $x=0.5, 1, 2, 3, 5$  at%) phosphors, were located in the white region. The chromaticity coordinates for  $\text{Cd}_{0.95}\text{Dy}_{0.05}\text{Ta}_2\text{O}_6$  phosphor is close to the standard equal energy white light ( $x=0.3351, y=0.3780$ ) illuminate. The color purity of the phosphors are interpreted by the Eq. (2) [23]:

$$\text{Color purity} = \frac{\sqrt{(x-x_i)^2 + (y-y_i)^2}}{\sqrt{(x_d-x_i)^2 + (y_d-y_i)^2}} \times 100 \quad (2)$$

where the CIE coordinates of the  $\text{Cd}_{1-x}\text{Ta}_2\text{O}_6:\text{xDy}^{3+}$  ( $x=0.5, 1, 2, 3, 5$  at%) phosphors are  $(x, y)$ , the CIE coordinates at the dominant wavelength of 579.2 nm are  $(x_d=0.509,$

$y_d=0.492)$ , the CIE coordinates of the standard white illumination are  $(x_i=0.313, y_i=0.329)$ . According to the Eq. (2), the color purity was estimated between 15.74–38.0%. The decrease in the color purity value is associated with the increase in the white light purity value [23]. The color purity of  $\text{Cd}_{0.95}\text{Dy}_{0.05}\text{Ta}_2\text{O}_6$  phosphor is 21.10%, which means being fairly close to white light. The color purities of the phosphors are given in Table 1. Further, in order to examine the quality of white light, the color correlated temperature (CCT) values were calculated by McCamy Eq. (2) [24]:

$$\text{CCT} = -449n^3 + 3525n^2 - 6823n + 5520.33 \quad (3)$$

where  $n = (x-x_e)/(y-y_e)$  is the inverse slope line, and  $x_e = 0.332$  and  $y_e = 0.186$ . The color correlated temperature (CCT) parameters at different concentrations were presented Table 1. Generally, the preferred CCT parameters range from 3500 to 6500 K, but the range from 3000 to 7800 K is also acceptable. The CCT values for the  $\text{Cd}_{1-x}\text{Ta}_2\text{O}_6:\text{xDy}^{3+}$  ( $x=0.5, 1, 2, 3, 5$  at%) phosphors were obtained in the range of 4556–5820 K. The estimated CCT data of all the samples located nearly in the daylight region. The CCT value for  $\text{Cd}_{0.95}\text{Dy}_{0.05}\text{Ta}_2\text{O}_6$

**Table 1.** CIE color coordinates color purities, and CCT parameters of  $\text{Cd}_{1-x}\text{Ta}_2\text{O}_6:\text{xDy}^{3+}$  ( $x=0.5, 1, 2, 3, 5$  at%) polycrystalline phosphors at different  $\text{Dy}^{3+}$  concentrations with the excitation of 353.2 nm.

Sample	The sample name in CIE diagram	FWHM		Color purity (%)	CCT (K)
		x	y		
$\text{Cd}_{0.995}\text{Dy}_{0.005}\text{Ta}_2\text{O}_6$	A	0.3499	0.3738	22.79	4902
$\text{Cd}_{0.99}\text{Dy}_{0.01}\text{Ta}_2\text{O}_6$	B	0.3519	0.3768	24.19	4847
$\text{Cd}_{0.98}\text{Dy}_{0.02}\text{Ta}_2\text{O}_6$	C	0.3242	0.3675	15.84	5820
$\text{Cd}_{0.97}\text{Dy}_{0.03}\text{Ta}_2\text{O}_6$	D	0.3663	0.4098	38.00	4556
$\text{Cd}_{0.95}\text{Dy}_{0.05}\text{Ta}_2\text{O}_6$	E	0.3351	0.3780	21.10	5411

### CIE 1931

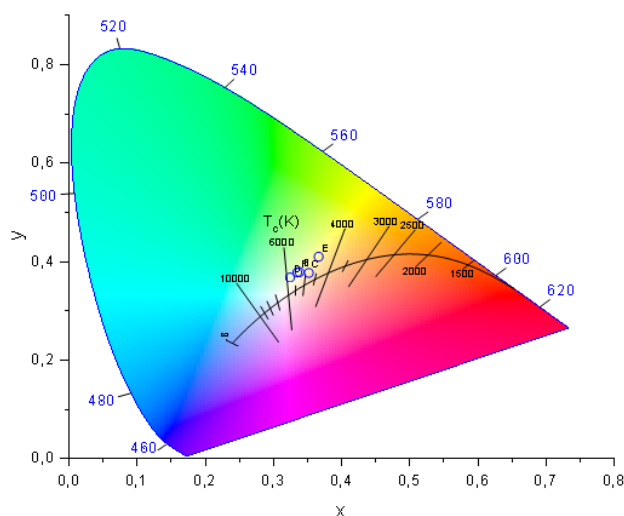


**Figure 7.** CIE diagram of  $\text{Cd}_{1-x}\text{Ta}_2\text{O}_6:\text{xDy}^{3+}$  ( $x=0.5, 1, 2, 3, 5$  at%) phosphors excited at  $\lambda_{\text{ex}}=352.2$  nm.

phosphor is 5411 K which located in the direct sun (noon)/daylight (sun&sky) or the midday sunlight region.

## Conclusion

The effect of charge balance on luminescence was investigated by synthesizing of  $\text{Cd}_{1-x}\text{Ta}_2\text{O}_6:x\text{Dy}^{3+}$  ( $x=0.5, 1, 1, 3, 5$  at%) phosphors with standard solid state method. XRD results of  $\text{Cd}_{1-x}\text{Ta}_2\text{O}_6:x\text{Dy}^{3+}$  ( $x=0.5, 1, 2, 3, 5$  at%) samples confirmed orthorhombic (orthorhombic) the presence and a formation of a single phase up to  $x=5$  at% concentration. SEM analysis showed that the grains have oval shape and grain size for all powders vary from submicron to a few microns. The photoluminescence of  $\text{Cd}_{1-x}\text{Ta}_2\text{O}_6:x\text{Dy}^{3+}$  ( $x=0.5, 1, 2, 3, 5$  at%) phosphors exhibited blue emission and yellow emission with the  ${}^4\text{F}_{9/2} \rightarrow {}^6\text{H}_{15/2}$  and  ${}^4\text{F}_{9/2} \rightarrow {}^6\text{H}_{13/2}$  transitions, respectively. The emission intensity of phosphors increased with the  $\text{Dy}^{3+}$  concentration, and did not form the phenomena of concentration quenching due to the improvement in the charge balance which reduced the structural defects and increased the excitation energy efficiency. The CIE values of the phosphors were found near white light point while CCT parameters located in the daylight region. Low color purities indicated closeness to white light. The CIE coordinates, color purity and color temperature (CCT parameter) of  $\text{Cd}_{0.95}\text{Dy}_{0.05}\text{Ta}_2\text{O}_6$  phosphor are  $x=0.3351$ ,  $y=0.3780$ , 21.10%, and 5411 K (the midday sunlight region), respectively. Based on the photoluminescence results, it was concluded that the  $\text{Cd}_{1-x}\text{Ta}_2\text{O}_6:x\text{Dy}^{3+}$  ( $x=0.5, 1, 2, 3, 5$  at%) phosphors have potential for white LEDs applications.

## References

- European Coordination Committee of the Radiological, Electromedical and Healthcare IT Industry, COCIR application for new exemption Page 1-12, Blvd A. Reyers 80 1020 Brussels, 2011.
- V.L. Colvin, M.C. Schlamp, A.P. Alivisatos, *Nature* 370 (1994) 354–357.
- L.E. Chaar, L.A. Lamont, N.E. Zein, *Renewable and Sustainable Energy Reviews* 15 (2011) 2165–75.
- A.I. Iorgu, D. Berger, L. Alexandrescu, B.S. Vasile, C. Matei, *Chalcogenide Letters* 10 (2013) 525 – 531.
- I. Willner, R. Baron, B. Willner, *Biosens. Bioelectron.* 22 (2007) 1841.
- Y.J. Choi, Y.J. Kim, J.W. Lee, Y. Lee, Y.B. Lim, H.W. Chung, *Journal of Nanoscience and Nanotechnology* 12 (2012) 2160–2168.
- Y. Su, Y. He, H. Lu, L. Sai, Q. Li, W. Li, L. Wang, P. Shen, Q. Huang, C. Fan, *Biomaterials* 30 (2009) 19–25.
- M. İlhan, M. K. Ekmekçi, Synthesis and photoluminescence properties of  $\text{Dy}^{3+}$  doped white light emitting  $\text{CdTa}_2\text{O}_6$  phosphors, *J. Solid State Chem.* 226 (2015) 243–249.
- M. İlhan, Synthesis, structural characterization, and photoluminescence properties of TTB-type  $\text{PbTa}_2\text{O}_6:\text{Eu}^{3+}$  phosphor *Int. J. Appl. Ceram. Technol.* 14 (2017) 1144–1150.
- M.K. Ekmekçi, M. İlhan, L.F. Güleriyüz, A. Mergen, Study on molten salt synthesis, microstructural determination and white light emitting properties of  $\text{CoNb}_2\text{O}_6:\text{Dy}^{3+}$  phosphor, *Optik* 128 (2017) 26–33.
- R. Erdem, M. İlhan, M.K. Ekmekçi, Ö. Erdem, Electrospinning, preparation and photoluminescence properties of  $\text{CoNb}_2\text{O}_6:\text{Dy}^{3+}$  incorporated polyamide 6 composite fibers, *Appl. Surf. Sci.* 421 (2017) 240–246.
- M. İlhan, M. Ekmekçi, A. Mergen, C. Yaman, Photoluminescence characterization and heat treatment effect on luminescence behavior of  $\text{BaTa}_2\text{O}_6:\text{Dy}^{3+}$  phosphor, *Int. J. Appl. Ceram. Technol.* 14 (2017) 1134–1143.
- M. İlhan, İ.Ç. Keskin, Analysis of Judd–Ofelt parameters and radioluminescence results of  $\text{SrNb}_2\text{O}_6:\text{Dy}^{3+}$  phosphors synthesized via molten salt method, *Phys. Chem. Chem. Phys.* 22 (2020) 19769–19778.
- M. İlhan, İ.K. Keskin, S. Gültekin, Assessing of photoluminescence and thermoluminescence properties of  $\text{Dy}^{3+}$  doped white light emitter TTB-lead metatantalate phosphor, *J. Electron. Mater.* 49 (2020) 2436–2449.
- M. İlhan, İ.Ç. Keskin, Photoluminescence, radioluminescence and thermoluminescence properties of  $\text{Eu}^{3+}$  doped cadmium tantalate phosphor, *Dalton Trans.* 47 (2018) 13939–13948.
- İ. Aritman, S. Yildirim, A. Kisa, L.F. Güleriyüz, M. Yurddaskal, T. Dikici, E. Celik, Synthesis and characterization of  $\text{Gd}_2\text{O}_2\text{SO}_4:\text{Pr}^{3+}$  scintillation material produced by sol–gel process for digital imaging system, *Acta Phys. Pol. A* 131 (2017) 106–108.
- M. Vukovic, L. Mancic, I. Dinic, P. Vulic, M. Nikolic, Z. Tan, O. Milosevic, The gadolinium effect on crystallization behavior and luminescence of  $\beta\text{-NaYF}_4:\text{Yb,Er}$  phase, *Int. J. Appl. Ceram. Technol.* 17 (2020) 1445–1452.
- R.S. Naorem, N.P. Singh, N.M. Singh, Photoluminescence studies of  $\text{Ce}^{3+}$  ion-doped  $\text{BiPO}_4$  phosphor and its photocatalytic activity, *Int. J. Appl. Ceram. Technol.* 17 (2020) 2744–2751.
- H. Yang, X. Liu, Z. Zhou, L. Guo, Preparation of a novel  $\text{Cd}_2\text{Ta}_2\text{O}_7$  photocatalyst and its photocatalytic activity in water splitting *Catal. Commun.* 31 (2013) 71–75.
- F. Haessner, G. Petzow, E. Preisler, Eignung von cadmiumtantalat als kontrollmaterial für hochtemperaturreaktoren, *J. Nucl. Mater.* 7 (1962) 46–57.
- G. Blasse, Energy transfer between inequivalent  $\text{Eu}^{2+}$  ions, *J. Solid State Chem.* 62 (1986) 207–211.
- G. Blasse, Energy transfer in oxidic phosphors, *Philips Res. Rep.* 24 (1969) 131.
- P. Sehrawat, A. Khatkar, P. Boora, M. Kumar, S. Singh, R.K. Malik, S.P. Khatkar, V. B. Taxak, Fabrication of single-phase  $\text{BaLaAlO}_4:\text{Dy}^{3+}$  nanophosphors by combustion synthesis, *Mater. Manuf. Process.* 35 (2020) 1259–1267.
- C.S. McCamy, Correlated color temperature as an explicit function of chromaticity coordinates, *Color Res. Appl.* 17 (1992) 142–144.